Electronic Supplementary Information

Photochemical hydrogen production based on HCOOH/CO_2 cycle promoted by pentanulear cobalt complex

Takuya Akai,[a] Mio Kondo,[a, b, c] Yutaka Saga[a, c] and Shigeyuki Masaoka*[a, c]

a. Division of Applied Chemistry, Graduate School of Engineering, Osaka University, 2-1 Yamadaoka, Suita, Osaka 565-0871, Japan.
b. JST, PRESTO, 4-1-8 Honcho, Kawaguchi, Saitama 332-0012, Japan.
c. Innovative Catalysis Science Division, Institute for Open and Transdisciplinary Research Initiatives (ICS-OTRI), Osaka University, Suita, Osaka 565-0871 Japan.

E-mail: masaoka@chem.eng.osaka-u.ac.jp

Table of Contents

Materials and Methods

Materials

$Ir(ppy)_3$, formic acid, trifluoroacetic acid and all the solvents except for *N,N*-dimethylacetamide (DMA) were purchased from FUJIFILM Wako Pure Chemical Corporation. Tetra-*n*-butylammonium perchlorate (TBAP), methyl iodide and DMA were purchased from Tokyo Chemical Industry Co., Ltd. $[Ir(dtbbpy)(ppy)_2](PF_6)$ and $[Ir(dF(CF_3)ppy)_2(dtbbpy)](PF_6)$ was purchased from Aldrich. All the reagents were of highest quality available and were used as received except for TBAP. TBAP was recrystallised from absolute ethanol. H_2O was purified using a Millipore MilliQ purifier. A pentanuclear cobalt complex (**Co5**) was prepared according to our previously reported procedures.[S1] 1,3-dimethyl-2-phenyl-2,3-dihydro-1*H*-benzo[d]imidazole (BIH) was synthesized using the slighly modified procedure reported in the literature.[S2]

Electrochemical studies

Cyclic voltammetry was performed with a Bio-Logic-Science Instruments potentiostat interfaced to a computer with SP-50 software, at room temperature under Ar using one-compartment cell with a standard three-electrode configuration, which consisted of a glassy carbon disk (diameter 3 mm, from BAS Inc.), a Ag/Ag^+ couple, and a platinum wire as the working, reference and auxiliary electrodes, respectively. The working electrode was treated between scans by means of polishing with 0.05 μm alumina paste (from BAS Inc.) and washing with purified H_2O. Ferrocene was used as an internal standard, and all potentials reported within this work are referenced to the ferrocenium/ferrocene couple at 0 V.

Photocatalytic reaction

For a typical run, a solution of DMA (2.0 mL) containing 30 μM **Co5**, 150 μM $Ir(ppy)_3$, 0.10 M BIH and formic acid (13 mM, 500 *eq. vs.* **Co5**) was purged with Ar for 15 minutes unless otherwise stated. The solution was then irradiated with a blue LED (wavelength $\lambda = 420$ nm) at 20 °C in a custom-made aluminium box with cooling system. The amounts of H_2 and CO_2 produced at the headspace of the cell was quantified by a Shimadzu GC-2014 with a TCD detector equipped with a packed column with Molecular Sieve 5A (Ar carrier gas, 40 °C) and a packed column with Active Carbon 60/80 (He carrier gas, 80 °C), respectively. Calibration curves were obtained by sampling known amounts of H_2 and CO_2.

Hydrogen evolution under CO_2 atmosphere

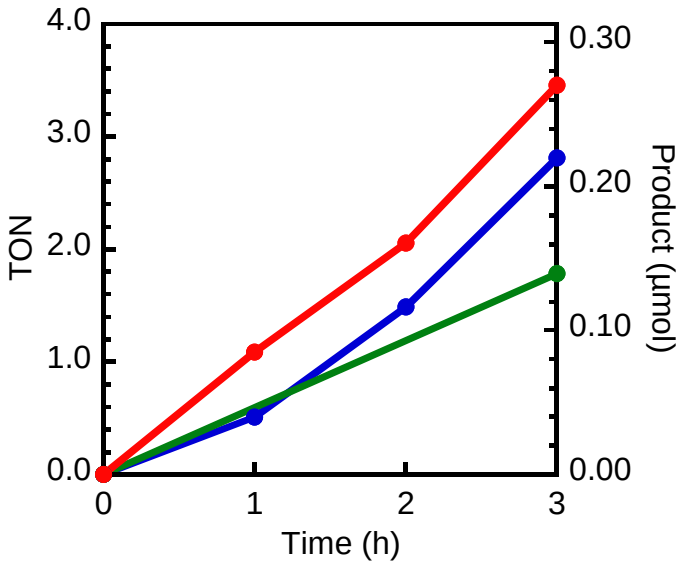

Figure S1. Photocatalytic production of CO (red line), HCOOH (green line) and H_2 (blue line) in a CO_2 saturated DMA/trifluoroethanol (17:3, v/v) solution containing 30 µM **Co5**, 150 µM $Ir(ppy)_3$ and 0.1 M BIH under irradiation of visible light (blue LED, wavelength λ = 420 nm).

Photochemical formic acid dehydrogenation reaction catalyzed by Co5

Table S1. Control experiments for photocatalytic formic acid dehydrogenation reaction by **Co5**.[a]

No.	[Co5] (μM)	[Ir(ppy)$_3$] (μM)	[BIH] (M)	substrate	Light (nm)	TON_{H_2}
1	30	150	0.1	HCOOH	420	22
2	30	150	0.1	TFA[b]	420	0.03
3	-	150	0.1	HCOOH	420	trace
4	30	-	0.1	HCOOH	420	0
5	30	150	-	HCOOH	420	0
6	30	150	0.1	HCOOH	dark	trace

[a] All experiments were carried out in DMA solution at 20 °C.

[b] TFA = trifluoroacetic acid.

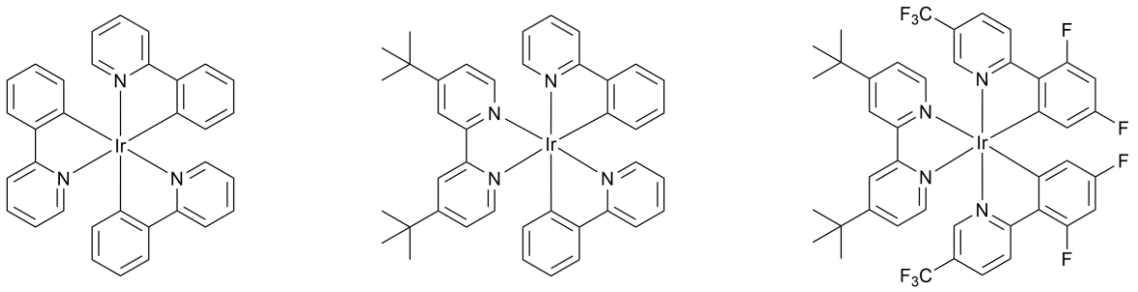

$Ir(ppy)_3$ $[Ir(dtbbpy)(ppy)_2](PF_6)$ **Ir-2** $[Ir(dF(CF_3)ppy)_2(dtbbpy)](PF_6)$ **Ir-3**

Figure S2. Structures of Ir photosensitizers.

Table S2. Properties of $Ir(ppy)_3$, **Ir-2** and **Ir-3**.

Photosensitizer	$Ir(ppy)_3$	**Ir-2**	**Ir-3**
$E_{1/2}(Ir^{III}/Ir^{II})$ (V *vs.* Fc/Fc^+)[a]	− 2.64	− 1.87	− 1.74

[a]$E_{1/2}(Ir^{III}/Ir^{II})$ was determined from the results of cyclic voltammetry (CV). Standard conditions: 0.2 mM solutions of Ir complex under Ar in MeCN containing 0.1 M TBAP.

Table S3. Reported properties [S3,4,5]

Photosensitizer	$Ir(ppy)_3$	**Ir-2**	**Ir-3**
$E_{1/2}(Ir^{III}/Ir^{II})$ (V *vs.* SCE)	−2.20	−1.51	−1.37
$E_{1/2}(Ir^{IV}/Ir^{III}*)$ (V *vs.* SCE)	− 1.73	− 0.96	− 0.89
$E_{1/2}(Ir^{IV}/Ir^{III})$ (V *vs.* SCE)	0.78	1.21	1.69
E_{gap} (eV)	2.75	n/a	2.20
τ (ns)	1900	557	2300

Assignment of redox peaks of Co5

The redox peaks of **Co5** were assigned by comparing the CV of **Co5** with those of heterometallic pentanuclear metal complexes, that composed of Hbpp, ruthenium ions at apical positions, and first-raw transition metal ions at the triangular core[S6]. The CVs of **Co5** and heterometallic pentanuclear metal complexes are shown in Figure S3. The heterometallic complex bearing ruthenium and zinc ions (**Ru_2Zn_3**, Figure S3a) exhibited two reversible redox waves at $E_{1/2}$ = 0.35 and 0.51 V (vs. ferrocene/ferrocenium (Fc/Fc^+)), and these waves were attributed to the sequential oxidation of the ruthenium ions at the apical positions because zinc ions are redox inactive. In the CVs of heterometallic complex bearing ruthenium and cobalt ions (**Ru_2Co_3**) and **Co5** (Figure S3b), two reversible oxidation and three reversible reduction waves were observed. The $E_{1/2}$ values of the oxidation waves of **Ru_2Co_3** (0.36 and 0.52 V) are almost identical to those of **Ru_2Zn_3**, indicating that these can be attributed to the oxidation of the ruthenium ions. The redox potentials of the reduction waves of **Ru_2Co_3** and **Co5** were also quite similar ($E_{1/2}$ = −1.71, −1.98, and −2.24 V for **Ru_2Co_3** and −1.72, −1.96, and −2.19 V for **Co5**), and thus, these waves are assignable to the reduction of the cobalt ions in the triangular core.

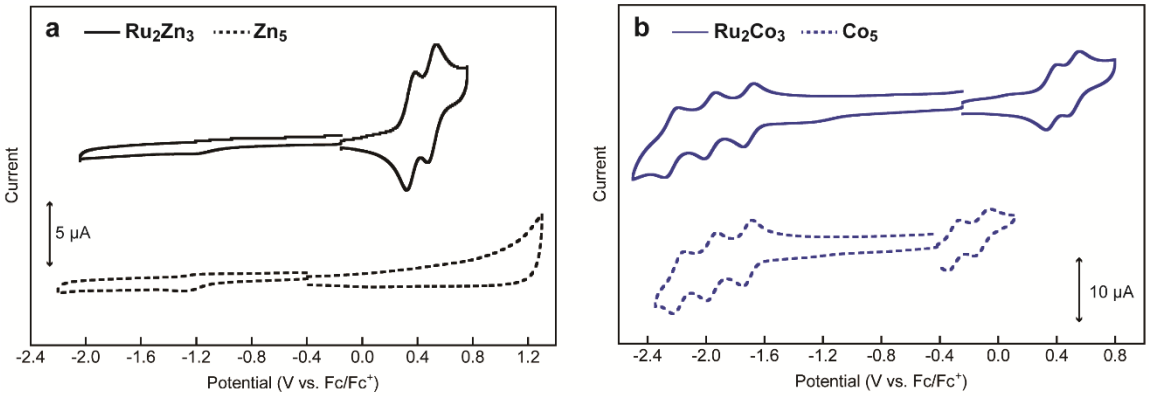

Figure S3. Cyclic voltammograms of a series of heterometallic (solid lines) and homometallic (dashed lines) pentanuclear metal complexes (0.2 mM) in acetonitrile solutions containing (n-Bu)$_4$NClO$_4$ (TBAP, 0.1 M) at a scan rate of 100 mV/s; (a) **Ru_2Zn_3** and **Zn_5** and (b) **Ru_2Co_3** and **Co_5**

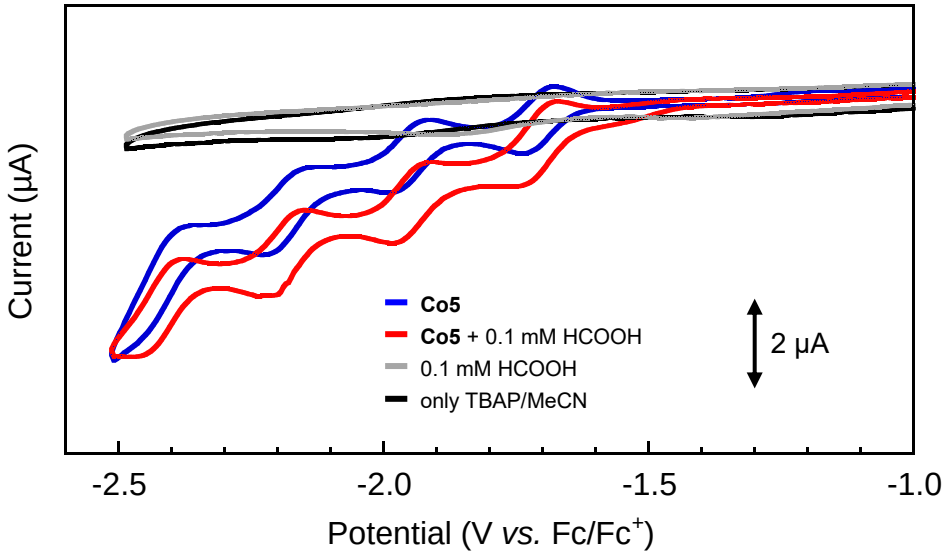

Figure S4. Cyclic voltammograms of 0.2 mM solution of **Co5** in the presence (red line) and in the absence (blue line) of 0.5 *eq.* formic acid in acetonitrile containing 0.1 M TBAP. The CVs were measured using a GC electrode at a scan rate of 10 mV s^{-1}.

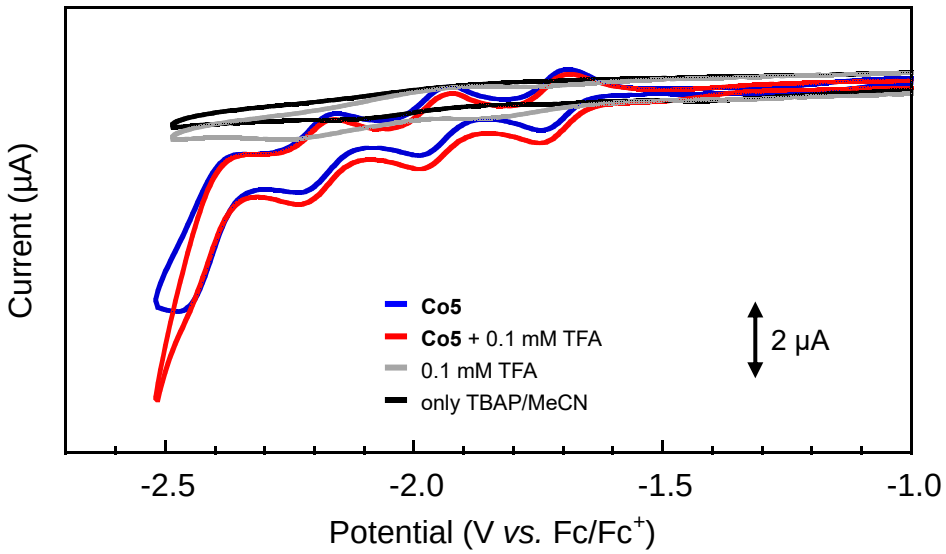

Figure S5. Cyclic voltammograms of 0.2 mM solution of **Co5** in the presence (red line) and in the absence (blue line) of 0.5 *eq.* trifluoroacetic acid in acetonitrile containing 0.1 M TBAP. The CVs were measured using a GC electrode at a scan rate of 10 mV s^{-1}.

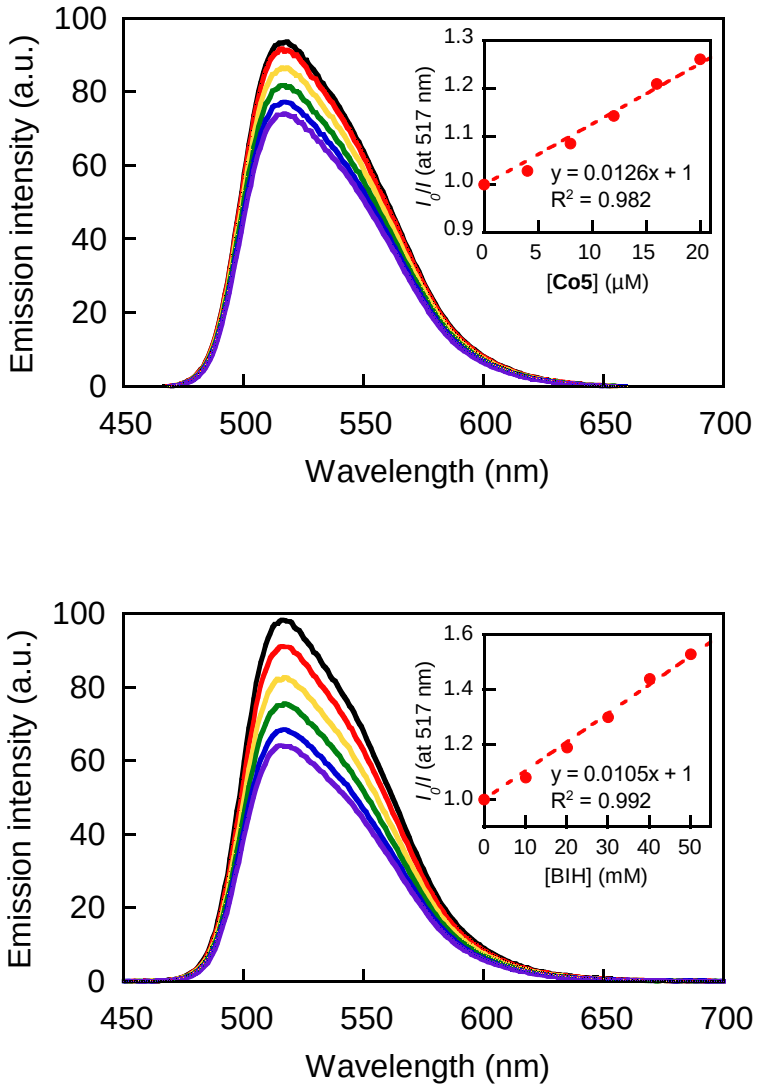

Figure S6. $Ir(ppy)_3$ emission quenching after excitation at 420 nm. (a) Upon increasing concentration of **Co5** in a 150 μM *N,N*-dimethylacetamide solution of $Ir(ppy)_3$. (b) Upon increasing concentration of BIH in a 150 μM *N,N*-dimethylacetamide solution of $Ir(ppy)_3$. (insets) Results of Stern-Volmer analyses, where I_0/I is the emission intensity without quencher (I_0) divided by the emission intensity with a known concentration of quencher (I). Luminescence spectra was recorded on Shimadzu RF5300PC spectrofluorophotometer.

UV-vis absorption spectrum of Co5

Molar absorption coefficients of **Co5** and $Ir(ppy)_3$ at 420 nm are 1943 and 5179 $M^{-1}cm^{-1}$, respectively. As the concentrations of **Co5** and $Ir(ppy)_3$ used in the quenching experiments are 30×10^{-6} and 150×10^{-6} M with optical path length of 1 cm, respectively, the absorbance at 420 nm is calculated to be 0.058 for **Co5** and 0.78 for $Ir(ppy)_3$. These results indicate that inner filter effect caused by **Co5** is relatively low (less than 7%).

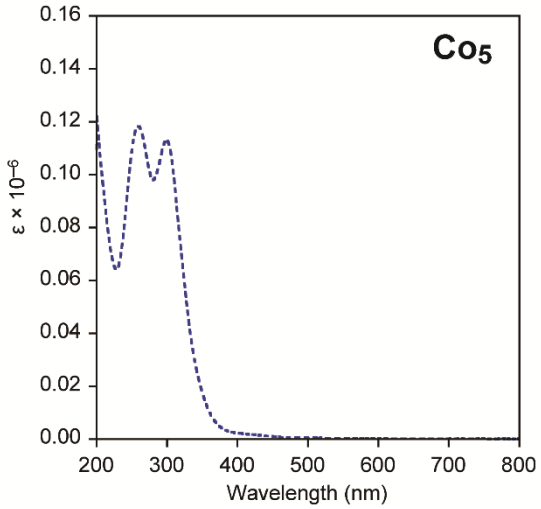

Figure S7. UV-vis absorption spectum of **Co5** (5 μM) in MeCN.

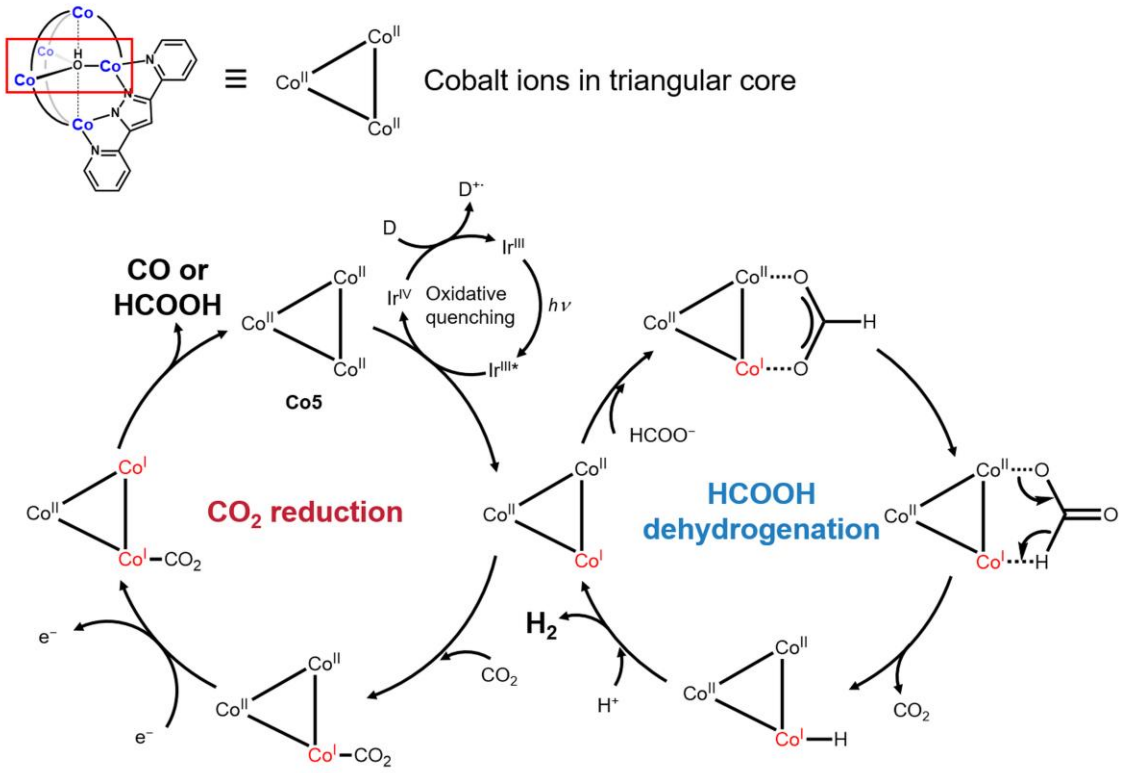

Scheme S1. Proposed mechanism of the dual catalysis process mediated by **Co5**. Dehydrogenation of formic acid (right) and two-electron reduction of CO_2 (left)

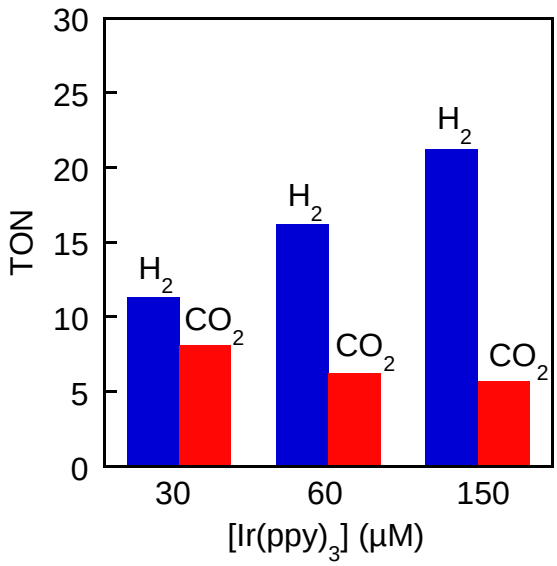

Figure S8. Products of photochemical formic acid dehydrogenation in a DMA solution containing 30 μM **Co5**, 30- 150 μM $Ir(ppy)_3$ and 0.1 M BIH.

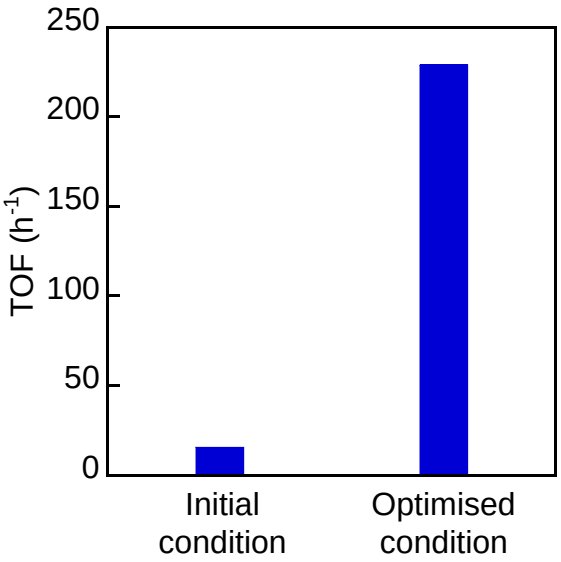

Figure S9. Turnover frequencies of the initial and optimized reactions at 20 °C. Reactions were performed in DMA solution containing (initial condition) 30 μM **Co5**, 150 μM $Ir(ppy)_3$, 100 mM BIH and 13 mM formic acid under irradiation with blue LED (420 nm) and (optimised condition) 30 μM **Co5**, 150 μM $Ir(ppy)_3$, 25 mM BIH and 25 mM formic acid under irradiation with Xe lamp ($420 \leq \lambda \leq 750$ nm).

Table S4. Comparison of catalytic activity of the relevant catalysts for photochemical formic acid dehydrogenation.

catalyst	Concentration	Temp. (°C)	TON (time)	TOF (h^{-1})[a]	Ref.
Co5	0.03 mM	r.t.	229 (1 h)	229	This work
$[CoH\{PPh(OEt)_2\}_4]$	20 mM	30	3.06 (6 h)	0.51	S7
$Fe_3(CO)_{12}/PPh_3$/tpy	(3 mM)	25	8.1 (3h)	2.7	S8
$Fe_3(CO)_{12}/PPh_3$/phen	(3 mM)	60	126 (24h)	5.2	S8
$Ir_2H_5(xylBINAP)_2(BF_4)$ (**4**)	3 mol%	r.t.	280 (24 h)	12	S9
[Cp*Ir(bpy-OMe)(Cl)](Cl) (**5**)	0.37 mM	r.t.	~500 (30 h)	~17	S10

[a] The turnover frequency (TOF, h^{-1}) was calculated by dividing the turnover number (TON) with duration of photoirradiation.

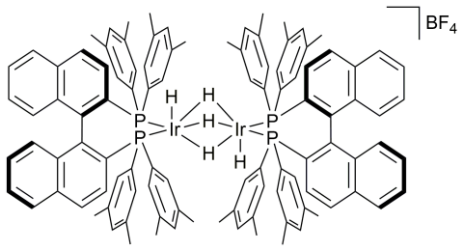

4

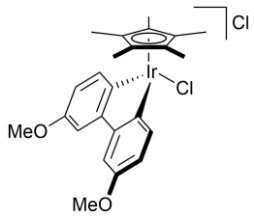

5

Figure S10. Molecular structures of photocatalysts for formic acid dehydrogenation (**4** and **5**) shown in Table S4.

Reference

S1. T. Akai, M. Kondo, S. K. Lee, H. Izu, T. Enomoto, M. Okamura, Y. Saga and S. Masaoka, *Dalton Trans.*, 2020, **49**, 1384.

S2. D. Hong, Y. Tsukakoshi, H. Kotani, T. Ishizuka and T. Kojima, *J. Am. Chem. Soc.*, 2017, **139**, 6538.

S3. K. Teegardin, J. I. Day, J. Chan and J. Weaver, *Org. Process Res. Dev.*, 2016, **20**, 1156.

S4. M. S. Lowry, J. I. Goldsmith, J. D. Slinker, R. Rohl, R. A. Pascal, G. G. Malliaras and S. Bernhard, *Chem. Mater.*, 2005, **17**, 5712.

S5. A. Singh, K. Teegardin, M. Kelly, K. S. Prasad, S. Krishnan and J. D. Weaver, *J. Organomet. Chem.*, 2015, **776**, 51.

S6. H. Izu, M. Kondo, M. Okamura, M. Tomoda, S. K. Lee, T. Akai, V. K. K. Praneeth, M. Kanaike, S. Kawata and S. Masaoka, *ChemRxiv Preprint*, DOI: 10.33774/chemrxiv-2021-n3jtl.

S7. M. Onishi, *J. Mol. Catal.*, 1993, **80**, 145.

S8. A. Boddien, B. Loges, F. Gärtner, C. Torborg, K. Fumino, H. Junge, R. Ludwig and M. Beller, *J. Am. Chem. Soc.*, 2010, **132**, 8924.

S9. Y. Sofue, K. Nomura and A. Inagaki, *Chem. Commun.*, 2020, **56**, 4519.

S10. S. M. Barrett, S. A. Slattery and A. J. M. Miller, *ACS Catal.*, 2015, **5**, 6320.